Spectroscopic and Theoretical Study of the Dimeric Dicationic Fullerene Complex $[(C_{70})_2]^{2+}(Ti_3Cl_{13})^-_2$

Alexey A. Popov,*,†,‡ Alexander V. Burtsev,† Vladimir M. Senyavin,† Lothar Dunsch,‡ and Sergey I. Troyanov†

Chemistry Department, Moscow State University, Moscow 119992, Russia, and Group of Electrochemistry and Conducting Polymers, Leibniz-Institute for Solid State and Materials Research Dresden, D-01171 Dresden, Germany

Received: June 15, 2008; Revised Manuscript Received: October 23, 2008

The first spectroscopic characterization of the dimeric dicationic fullerene complex $[(C_{70})_2]^{2+}(Ti_3Cl_{13})^-_2$ is reported and supported by DFT calculations. The IR spectrum of the dimer is interpreted in terms of the normal modes of the pristine C_{70}, and the effects of charging C_{70} and the intercage bond formation between C_{70} units on the IR spectrum are discussed. Analysis of the vibrational spectrum of the anion, $Ti_3Cl_{13}^-$, is also provided. NIR absorption and fluorescence spectra of the complex are studied, and the dimer is shown to have a small HOMO−LUMO gap of 0.8 eV. The electronic structure of $[(C_{70})_2]^{2+}$ is studied with the use of DFT and compared to that of the other single-bonded fullerene dimers, including $[(C_{70})_2]^{2-}$, $(C_{69}N)_2$, and $[(C_{60})_2]^{2-}$. Characteristic features in the vibrational spectra and electronic structure of all single-bonded fullerene dimers are revealed.

Introduction

In a search for the halogenation agents for fullerenes, we unexpectedly found that a mixture of Br_2 and $TiCl_4$ is an effective chlorinating system allowing preparation of the new fullerene derivatives.[1] It was established that bromine concentration is critical to the composition of the reaction products.[2] For a reaction between C_{60} and $TiCl_4$ containing a high concentration of Br_2, $C_{60}X_{24}$ (X = Cl, Br) products were obtained with the Cl/Br ratio of 0.5 or higher. However, in the systems with lower Br_2 content, lower fullerene chlorides, $C_{60}X_6$ (X = Cl, Br), or a dimer, $(C_{60}Cl_5)_2$, have been isolated and structurally characterized.[2] Recently, the mixture of $TiCl_4$ and Br_2 was successfully used for chlorination of C_{76}[3] and C_{78}[4,5] thus resulting in the first chlorides of higher fullerenes, $C_{76}Cl_{18}$ and $C_{78}Cl_{18}$, investigated by single-crystal X-ray crystallography.[3−5]

The system C_{70}−$TiCl_4$−Br_2 provided further examples of the new fullerene derivatives. At higher bromine concentration, a new chloride, $C_{70}Cl_{16}$, with unprecedented addition pattern was isolated and investigated by X-ray crystallography.[1] It was assumed that the presence of a strong Lewis acid ($TiCl_4$) in the system resulted in a generation of Br^+ or BrCl species that could act as halogenating agents under simultaneous (or subsequent) halogen exchange. An entirely unanticipated complex has been prepared in the same system at very low bromine content. A reaction of $C_{70}Br_{10}$ with excess $TiCl_4$ afforded the first isolation of an ionic complex, $[(C_{70})_2]^{2+}(Ti_3Cl_{13})^-_2$, containing a singly bonded dimeric dication, $[(C_{70})]^{2+}$ (Figure 1), and a trinuclear chlorotitanate anion, $(Ti_3Cl_{13})^-$, both species having been observed for the first time.[2] It should be noted that cationic fullerenes are difficult to obtain due to high ionization potential of fullerene molecules. For instance, the oxidation $E_{1/2}$ potentials of C_{60} and C_{70} are as high as 1.26 and 1.20 V (vs Fc/Fc^+), respectively.[6] Known "all-carbon" cations were isolated as radical cations $[C_{60}^+]$ and $[C_{76}^+]$ in the salts with carborane anions $[CB_{11}H_6X_6]^-$ (X = Cl, Br) and investigated by means of EPR, IR, and NIR spectroscopies.[7−9] Therefore, the isolation of the cationic species of C_{70} under weakly oxidizing conditions, but rather due to a very high Lewis acidity of the media assisting the formation of stable anion, is quite remarkable (note that the nature of the oxidizing agents in this system is still not clear). On the other hand, formation of the anionic fullerene species is favored by high electron affinities of both C_{60} and C_{70}. Therefore, both radical anions (C_{60}^- and C_{70}^-) in fullerides[9] and singly bonded anionic dimers, $[(C_{60})_2]^{2-}$ and $[(C_{70})_2]^{2-}$, can be isolated.[10−14] Significantly, as C_{70} has five inequivalent types of atoms, up to 15 different isomers of single-bonded $(C_{70})_2$ dimers are possible.

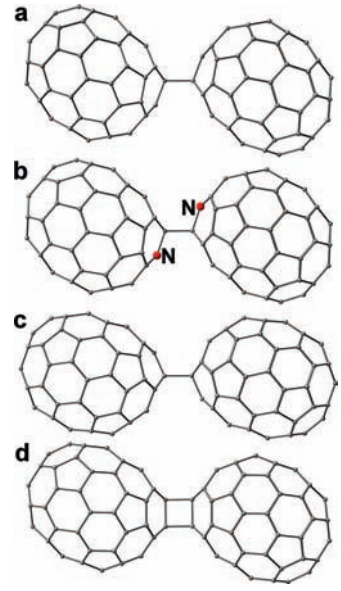

Figure 1. Molecular structures of (a) $[(C_{70})_2]^{2+}$, (b) isostructural $(C_{69}N)_2$, (c) $[(C_{70})_2]^{2-}$, and (d) neutrally charged $(C_{70})_2$.

* To whom correspondence should be addressed. E-mail: popov@phys.chem.msu.ru.
† Moscow State University.
‡ Leibniz-Institute for Solid State and Materials Research Dresden.

10.1021/jp805264q CCC: $40.75
Published on Web 12/08/2008

However, only one isomer is found for $[(C_{70})_2]^{2+}$.[2] Moreover, a single but *different* isomer is found for $[(C_{70})_2]^{2-}$.[12] At the same time, for $(C_{69}N)_2$, which is isoelectronic to $[(C_{70})_2]^{2-}$, four isomers were isolated,[15,16] including those corresponding to the bonding motif of $[(C_{70})_2]^{2-}$, $[(C_{70})_2]^{2+}$, and their combination.[17,18]

In this article we report on the synthesis and spectroscopy of $[(C_{70})_2]^{2+}(Ti_3Cl_{13})^-_2$ and present a comparative theoretical study of singly bonded dimeric dicationic and dianionic $(C_{70})_2$ species as well as their heterofullerene analogue, $(C_{69}N)_2$.

Experimental Details

The synthetic route to $[(C_{70})_2]^{2+}(Ti_3Cl_{13})^-_2$ in this work was modified in that C_{70} fullerene was used instead of $C_{70}Br_{10}$ as described earlier.[2] C_{70} (20 mg, 0.023 mmol) and $TiCl_4$ (0.5−0.6 mL) were placed into a glass ampule. One drop of dry Br_2 (ca. 0.05 mL, 1.30 mmol) was added and the ampule was evacuated and sealed. After the ampule was heated at ca. 100 °C for 2−3 days, black crystals were deposited on the ampule's walls. They were separated from excess $TiCl_4$ by decanting and additionally dried in vacuo. Determination of the unit cell parameters for single crystals by X-ray crystallography confirmed formation of the $[(C_{70})_2]^{2+}(Ti_3Cl_{13})^-_2$ (triclinic unit cell parameters found in this work, $a = 10.192$ Å, $b = 13.788$ Å, $c = 16.713$ Å, $\alpha = 86.190°$, $\beta = 89.034°$, $\gamma = 79.508°$, are very close to those reported for $[(C_{70})_2]^{2+}(Ti_3Cl_{13})^-_2$ in ref 2). The well-crystallized compound placed under paraffin oil decomposes only slowly (15−20 min) in air atmosphere. A mixture of $[(C_{70})_2]^{2+}(Ti_3Cl_{13})^-_2$ and dry NaCl was pressed into a pellet in a glovebox in an argon atmosphere. The pellet was quickly transferred to the Equinox-55 FT-IR spectrometer (Bruker, Germany) just before recording the IR-NIR spectrum (370−7000 cm^{-1} range, resolution 1 cm^{-1}, 128 scans). The spectra taken within the first hour did not show noticeable changes. However, at longer times decomposition of the complex became apparent, and only C_{70} absorption bands could be detected after exposure of the pellet in air for 24 h. For recording Raman and luminescence spectra, crystals of $[(C_{70})_2]^{2+}(Ti_3Cl_{13})^-_2$ were placed into thin-walled capillaries which were then sealed off immediately after taking them out of the glovebox. The spectra were measured with an FRA-106 Raman module attached to an Equinox-55 FT-IR spectrometer (excitation with the 1064 nm line of an Nd:YAG laser) and a Jobin Yvon T 64000 triple spectrometer (excitation with the 514.5 nm line of an Ar^+ laser).

Computational Details

Optimization of molecular structures and Hessian calculations were performed by using PBE functional[19] and TZ2P-quality basis set with {6,3,2}/(11s,6p,2d) contractation scheme implemented in the PRIRODA package.[20,21] The code employed expansion of the electron density in an auxiliary basis set to accelerate evaluation of the Coulomb and exchange-correlation terms.[20]

Results and Discussion

Vibrational Spectroscopy. Vibrational spectra of C_{70} were thoroughly studied by several groups, and their interpretation based on DFT calculations was provided.[22,23] As C_{70} has rather high D_{5h} symmetry, the limited number of its fundamentals is IR-active ($21E' + 10A_2''$ symmetry types), and though this number is much larger than in C_{60}, the spectra of C_{70} are still rather simple because only a few IR-active bands have high intensity (Figure 2). A removal of one electron from the fullerene and formation of the intercage bond(s) inevitably results in the lowering of the symmetry, and hence the spectra of the dimer should be much more complex. The monomeric C_{70} unit in C_{2h}-symmetric $[(C_{70})_2]^{2+}$ dimer retains only C_s site symmetry. Therefore, vibrational modes of the C_{70} units are transformed to A′ and A″ symmetry types, and in the dimer these vibrations transform to $104A_g + 100B_g + 100A_u + 104B_u$ modes (see Table 1 for the correlation of irreducible representations). Thus, all fundamentals of C_{70} lose their degeneracy and should produce IR and Raman active vibrations in the vibrational spectra of the dimer. The same symmetry situation is applicable to the neutral $(C_{70})_2$, which also has C_{2h} molecular symmetry,[24] and its spectra indeed were shown to be more complicated than those of the monomer. Formation of the intercage bond can also produce specific localized vibrations. Finally, charging the cage modifies its electronic structure, the effect of which can also reflect itself in the vibrational spectra. These issues are analyzed in detail in the following part of this section.

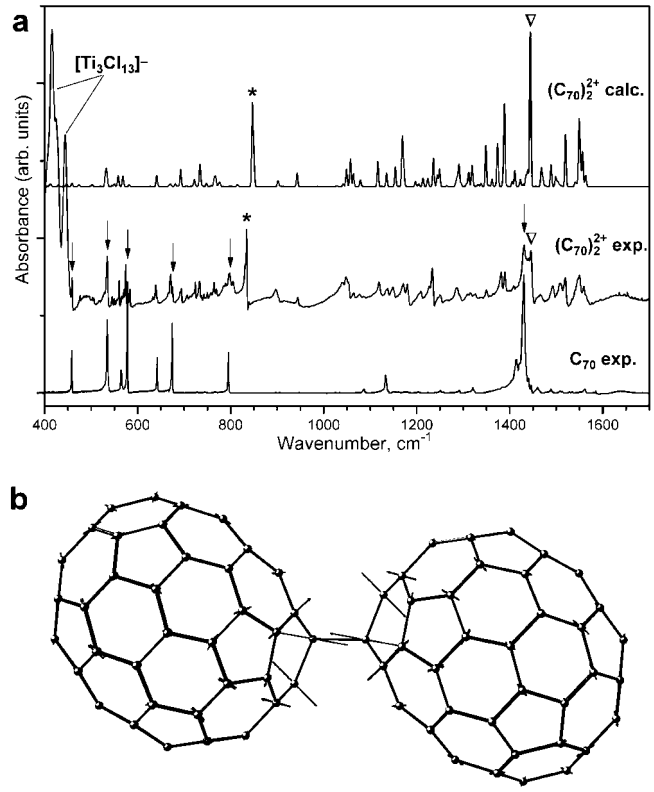

Figure 2. (a) Experimental and calculated IR spectra of $[(C_{70})_2]^{2+}$ and experimental IR spectrum of C_{70} (the arrows denote the lines in the experimental spectrum of the dimer which can be also assigned to C_{70}) and (b) displacement pattern for the characteristic IR mode of the intercage bond at 835 cm^{-1}

TABLE 1: Correlation of Irreducible Representations of D_{5h}, C_{2v}, C_s, and C_{2h} Groups

D_{5h}	C_{2v}[a]	C_s[b]	C_{2h} (dimer)	IR[c]	Raman[c]
A_1'	A_1	A′	$A_g + B_u$	0→1	1→1
A_2'	B_1	A″	$A_u + B_g$	0→1	0→1
E_1'	$A_1 + B_1$	A′ + A″	$A_g + B_g + A_u + B_u$	1→2	0→2
E_2'	$A_1 + B_1$	A′ + A″	$A_g + B_g + A_u + B_u$	0→2	1→2
A_1''	A_2	A″	$A_u + B_g$	0→1	0→1
A_2''	B_2	A′	$A_g + B_u$	1→1	0→1
E_1''	$A_2 + B_2$	A′ + A″	$A_g + B_g + A_u + B_u$	0→2	1→2
E_2''	$A_2 + B_2$	A′ + A″	$A_g + B_g + A_u + B_u$	0→2	0→2

[a] The symmetry of C_{70}^+. [b] Cite-symmetry of C_{70} in $[(C_{70})_2]^{2+}$. [c] The last two columns show activation and splitting pattern for C_{70} modes in $[(C_{70})_2]^{2+}$.

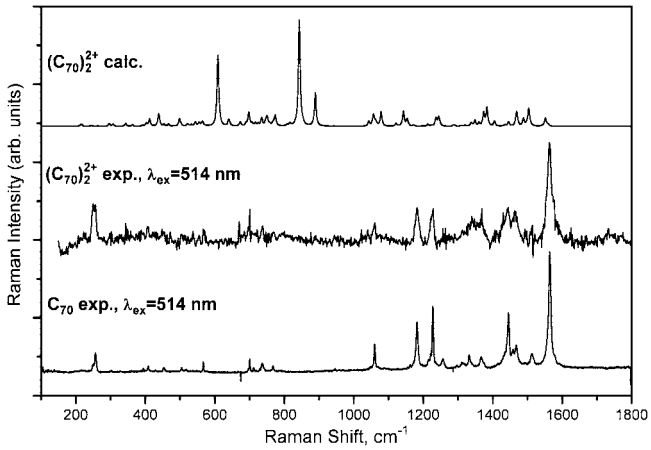

Figure 3. Experimental Raman spectrum of $[(C_{70})_2]^{2+}(Ti_3Cl_{13})^-_2$, compared to the Raman spectrum of C_{70} (λ_{ex} = 514 nm) and DFT-computed Raman spectrum of $[(C_{70})_2]^{2+}$.

Figure 2 shows the IR spectrum of the $[(C_{70})_2]^{2+}(Ti_3Cl_{13})^-_2$ complex as compared to the spectrum of C_{70} and to the DFT-computed spectrum of the $[(C_{70})_2]^{2+}$ dimer. By virtue of the comparably high mass of Ti and Cl atoms, absorption bands of the anion occur at low frequencies (below 450 cm^{-1}, see further discussion) and hence the spectrum in the medium-IR range can be attributed exclusively to the fullerene-based vibrations. Comparison to the spectrum of C_{70} has shown that the partial decomposition of the complex still took place, most probably initiated by the traces of water in NaCl used for the pellet formation. The bands which coincide in frequency to those of C_{70} and hence can be attributed to the parent fullerene are denoted by arrows in Figure 2 (note that the dimer can also have vibrational frequencies with the same wavenumbers). However, as the spectrum of C_{70} is substantially less rich, vibrational features of the cationic dimer can be determined unambiguously. The calculated spectrum of the $(C_{70})_2^{2+}$ dimer provides reasonable agreement with the experimental data, and hence can be used as a base for the detailed analysis.

Raman spectroscopic studies of the complex met severe difficulties due to the high fluorescence background and/or low sample stability under the laser irradiation. Thus, the use of the infrared laser (λ_{ex} = 1064 nm) for the excitation of the spectra resulted only in the luminescence background, which prevented the measurement of the Raman spectrum. When the 514 nm line of the Ar^+ laser was used, the sample was found to be unstable at the medium laser power, and only when very low laser power (0.07 mW) was applied did the sample exhibit long-term stability and afford the measurement of the Raman spectrum (however, due to the low intensity of the excitation laser, the signal-to-noise ratio is rather small). The spectrum was found to be very similar to the spectrum of C_{70} measured with the same excitation wavelengths, the only noticeable differences being additional features in the 1300−1500 cm^{-1} range and somewhat different intensity distribution. A dramatically different intensity distribution in the Raman spectrum of $[(C_{70})_2]^{2+}$ is predicted by DFT, which is not surprising because calculations predict nonresonant scattering intensities, while excitation of the spectrum in the visible range results in the preresonance Raman scattering. Though the possibility of dimer decomposition by the laser irradiation cannot be fully excluded, it should be noted that the Raman spectrum of $[(C_{70})_2]^{2-}$ in the Rb−C_{70} system also showed close similarity to the spectrum of C_{70}, while inelastic scattering measurement clearly indicated the presence of the intercage bonds in that sample (Figure 3).[25] However, in view of the close similarity of the spectra of C_{70} and the dimer causing ambiguity in the interpretation of the Raman spectra, further discussion of the influence of the dimerization and charging of C_{70} on the vibrational modes will be limited to the IR spectra and the results of DFT calculations.

Formation of the intercage bond forces some of the "external" degrees of freedom (i.e., translational and rotational) of the monomers to become vibrations of the dimer molecule. Such vibrations usually have low frequency (less than 150 cm^{-1}), and for the neutrally charged dimers of C_{60} and C_{70} as well as for $[(C_{60})_2]^{2-}$ some of them could be observed in the Raman spectra.[24,26,27] Unfortunately it was not possible to measure the Raman spectrum of $[(C_{70})_2]^{2+}$ in this range because of the strong background level, and so we will discuss these kinds of vibrations only from the theoretical point of view. As anticipated, DFT calculations predict six low-frequency (below 100 cm^{-1}) vibrations of the dimer originating from the frustrated rotations and translations of the monomer units. The modes with purely rotational character occur at 8 (A_u), 17 (A_u), and 19 (B_u) cm^{-1}, the stretching intercage mode is predicted at 64 cm^{-1} (A_g), and two modes with the mixed translational−rotational character are predicted at 81 (B_g) and 86 cm^{-1} (A_g). The modes with similar low frequencies are found for all single-bonded dimers considered in this work (see Table 2). The frequencies of these vibrations are systematically lower than predicted at the same level of theory for the neutrally charged $(C_{70})_2$, which can be readily explained by the stronger intercage linkage by two covalent bonds in $(C_{70})_2$. For the latter, cage "librations" occur at 18 (A_u), 21 (A_u), and 29 cm^{-1} (B_u), the A_g "stretching" mode is predicted at 80 cm^{-1}, and mixed translational−rotational vibrations occur at 114 (B_g) and 127 (A_g) cm^{-1}. Three latter modes can be identified in the experimental spectrum of $(C_{70})_2$ at 89, 117, and 129 cm^{-1},[24] respectively, in close agreement with the DFT-computed values.

In the mid-IR range, a specific vibration localized presumably at the intercage bond and the neighboring carbon atoms is found as a strong band at 833 cm^{-1} (846 cm^{-1} calcd, B_u symmetry type). Its atomic displacement pattern is visualized in Figure 2; this mode can be roughly described as a translational displacement of the intercage bond as a whole accompanied by the radial motions of the neighboring carbon atoms. Analysis of the IR spectra of single-bonded fullerene dimers available in the literature as well as DFT calculations performed in this work have shown that the vibrations of this sort are found for all single-bonded fullerene dimers in the 800−900 cm^{-1} range (see Table 2), and these modes always have high IR intensity. Note that usually this mode is partially mixed with the cage vibrations and hence has considerable contribution in two−three vibrations of the dimers. Earlier Andreoni et al.[28] predicted that such vibrations should appear in the spectrum of $(C_{59}N)_2$ at 850 cm^{-1}, and later they were indeed observed by Krause et al. as a multiplet of lines at 819/836/844 cm^{-1} with the strongest band at 844 cm^{-1}.[29] In the IR spectrum of the quenched Rb−C_{60} phase[30] comprised of $[(C_{60})_2]^{2-}$ dimers this mode can be attributed to the bands at 816 and 838 cm^{-1}, while in the IR spectra of $[(C_{70})_2]^{2-}$ we assign this mode to the strong band at 800 cm^{-1} and, with less confidence, to the medium intensity band at 842 cm^{-1}.[12,31] Finally, in the spectrum of b,b-$(C_{69}N)_2$ this mode is probably responsible for a band at 823 cm^{-1}.[17] In summary, the "tanslational" mode of the intercage bond in the single-bonded dimers always appears in the 800−900 cm^{-1} range with high IR intensity and can be used as the IR fingerprint of single-bonded fullerene dimers (Table 2).

TABLE 2: PBE/TZ2P Computed Inter-Cage Bond Lengths (Å), the Frequencies of the Characteristic Vibrations of the Single-Bonded Dimers (cm^{-1}), and Their Dimerization Energy (kJ mol^{-1})

		"translation", A_g		intercage, B_u		stretch, A_g	
	intercage bond, Å	exptl	calcd[a]	exptl	calcd[a]	calcd[a]	E_{dim}, kJ mol^{-1}
$[(C_{70})_2]^{2+}$	1.647		64	833	846, 850	843	100.6
$[(C_{70})_2]^{2-}$	1.634		65	800, 842[c]	831, 866	876, 897	95.7
a,a-$(C_{69}N)_2$	1.593		68		822, 865	983	−142.7
b,b-$(C_{69}N)_2$	1.597		66	823[d]	834, 910	977	−111.9
$[(C_{60})_2]^{2-}$	1.653	82[b]	69	816, 838[e]	845, 860	858	137.3
$(C_{59}N)_2$	1.596	88[b]	74	844[f]	840, 857	931, 992	−118.2

[a] All calculated values in the table are obtained in this work at the PBE/TZ2P level; [b] Reference 24. [c] References 9 and 28. [d] Reference 14. [e] Reference 27. [f] Reference 26.

In terms of the monomeric unit, this characteristic vibration of the intercage bond can be described as a radial displacement of the four-coordinated carbon atom. Given displacement in the two monomeric units occurs in the antiphase, the resulting vibration of the dimer is IR active and can be described as a translation of the intercage bond as a whole as already discussed above. On the contrary, if displacements in two monomeric units are in phase, the resulting vibration can be described as the A_g-symmetric stretching mode of the intercage bond (note that opposed to the lower frequency intercage stretching mode described above, here centers of mass of the monomeric units remain static). The latter is Raman active and expected at somewhat higher frequency than the "translational" mode (Table 2). Unfortunately, we could not identify this mode either in our spectrum or in the literature Raman spectra of $[(C_{60})_2]^{2-}$ and $(C_{59}N)_2$, presumably because of its low intensity.

To estimate the effect of the cage charging on the vibrational spectra, first we have computed the spectra of the C_{70}^+ cation. Unfortunately, experimental data on this ion are not available, and this discussion is inevitably limited to the computational results. As the HOMO of C_{70} is 2-fold degenerated, removing one electron from this orbital results in the Jahn−Teller distortion of the cation with the symmetry reduction from D_{5h} to C_{2v}. Indeed, optimization of the coordinates of C_{70}^+ without any symmetry constraints resulted in the C_{2v} symmetric structure for the cation. Figure 4 shows DFT-optimized bond lengths in C_{70}^+ as compared to those in C_{70} calculated at the same level of theory. As can be seen, the bond lengths in the cation are very close to those in the pristine C_{70}, the difference not exceeding 0.01 Å and in most cases being much smaller. Within the C_{2v} symmetry, degeneracy of C_{70} vibrations is lifted and therefore a splitting and mixing of the parent C_{70} modes can happen (see Table 1 for correlation between irreducible representations of D_{5h} and C_{2v} groups). Projecting vibrational eigenvectors of C_{70}^+ on the space of the vibrational eigenvectors of C_{70} has shown that the mixing is rather weak, and with few exceptions, vibrational eigenvectors of C_{70} are mostly preserved in the cation. This is a sensible result taking into account the small structural changes in C_{70} induced by the removal of one electron. The splitting of the *E*-type modes of C_{70} is also quite small, usually less than 10 cm^{-1}; however, in some cases the larger values are observed. The highest degree of splitting is found for the $E_1'(13)$ mode of C_{70} (calcd 1082 cm^{-1}, exptl 1087 cm^{-1}), which is split into 990 (B_2) and 1088 cm^{-1} (A_1) modes in the cation. This vibration can be described as a stretching mode of the longest C−C bonds at the equator of C_{70} (Figure 4). The other C_{70} vibrations with considerable degree of splitting in the cation are as follows: $E_1'(2)$ (calcd 360 cm^{-1}, exptl 361 cm^{-1}) → 332 (B_2) + 359 (A_1); $E_1''(11)$ (calcd 1057, exptl 1048) → 1027 (B_1) + 1058 (A_2); $E_1'(14)$ (calcd 1174, exptl 1176) → 1146 (B_2) + 1168 (A_1); $E_1'(20)$ (calcd 1475, exptl 1489) → 1450 (B_2) + 1482 (A_1); $E_1'(21)$ (calcd 1552, exptl 1557) → 1526 (B_2) + 1559 (A_1). The special case of splitting is the $E_2'(1)$ mode of C_{70} (calcd 219, exptl 225), which is largely responsible for the Jahn−Teller distortion of the cage in C_{70}^+. In the cation the frequency of one of its components is only 19 cm^{-1} (B_2), while another component occurs at the frequency of 214 cm^{-1} (A_1). As can be seen, in all *E*-symmetry modes subjected to considerable splitting upon charging of C_{70}, the A_1 (A_2) component retains the frequency of the parent C_{70} mode, while the B_2 (B_1) component is red-shifted.

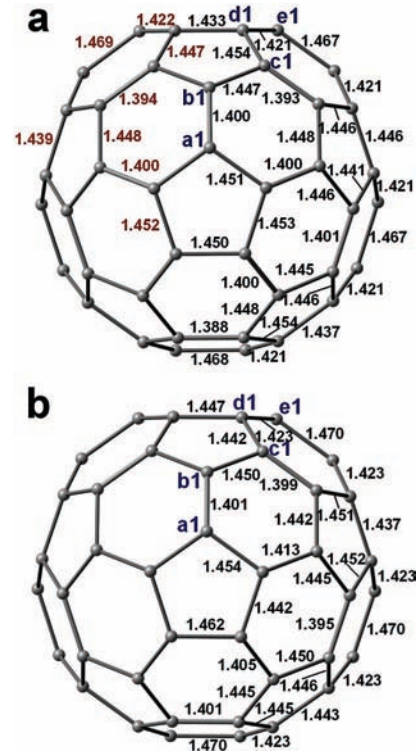

Figure 4. DFT-optimized bond lengths and atom numbering in C_{70}^+ (a) and C_{70}^- (b). The bond lengths in the neutral C_{70} optimized at the same level of theory are also shown in part a, highlighted with brown.

We could not find any systematic shift of the vibrational frequencies of the cation. For some modes, the frequencies are larger than in C_{70}, for others they are smaller, and there is no correlation between the shift and the frequency range (see Table S2 in the Supporting Information). For the majority of modes, vibrational frequencies in the cation lie within 10 cm^{-1} of the corresponding frequencies in C_{70}. This can be compared to the experimental data on C_{76}^+ and C_{76}, for which the shift of the vibrational frequencies also did not exceed 8 cm^{-1}.[8]

As to the IR spectrum of $[(C_{70})_2]^{2+}$, our projection analysis has shown that the most intense bands of the dimer originate

TABLE 3: Experimental and Selected[a] Calculated Vibrational Frequencies and Infrared Intensities in $[(C_{70})_2]^{2+}$ and Normal Mode Assignment

	calcd		exptl		
sym	ν, cm^{-1}	int, % [b]	ν, cm^{-1}	int [c]	assignment in terms of C_{70} modes {exptl/calcd, cm^{-1}}, % [d]
B_u	458.6	2.34	458	w, C_{70}	92 $A_2''(2)$ {458/457}
B_u	473.7	1.15	476	w	94 $E_1''(3)$ {480/476}
B_u	530.4	5.37	535	m, C_{70}	66 $E_1(5)$ {534/533}, 16 $E_2''(4)$ {−/518}, 14 $E_2'(5)$ {536/537}
A_u	532.3	6.34	535	m, C_{70}	78 $E_1(5)$ {534/533}, 14 $E_2'(5)$ {536/537}
B_u	533.8	4.11	535	m, C_{70}	70 $E_2'(5)$ {536/537}
A_u	534.6	1.21	535	m, C_{70}	82 $E_2'(5)$ {536/537}
A_u	544.8	0.63	545	w	88 $E_1''(5)$ {549/550}
B_u	549.8	1.91	550	w	72 $E_1''(5)$ {549/550}
B_u	557.6	5.91	560	w+	54 $A_1'(4)$ {568/563}, 38 $E_2''(5)$ {557/559}
B_u	558.8	2.01	560	w+	52 $E_2''(5)$ {557/559}, 24 $A_1'(4)$ {568/563}, 16 $A_2''(3)$ {564/563}
B_u	567.2	2.78	574	m	72 $A_2''(3)$ {564/563}, 14 $E_1(6)$ {578/573}
A_u	568.7	4.96	574	m	96 $E_1(6)$ {578/573}
B_u	581.7	1.16	583	w	76 $E_1(6)$ {578/573}
B_u	640.9	5.82	639	w+	94 $E_1(7)$ {642/643}
B_u	669.6	1.62	672	m	78 $E_1(8)$ {674/670}
B_u	692.2	11.36	694	w+	82 $A_2'(4)$ {695/694}
B_u	704.5	0.37	706	w	92 $E_2''(7)$ {702/704}
B_u	721.6	4.83	724	w+	78 $E_1''(7)$ {713/718}
B_u	733.7	12.96	733	w+	46 $E_1(9)$ {728/732}, 36 $E_2'(8)$ {727/734}
B_u	747.8	2.12	750	w	42 $E_2'(9)$ {737/737}, 18 $E_1''(8)$ {760/758}, 16 $E_1(10)$ {795/746}
B_u	764.5	5.50	764	w+	44 $E_2''(9)$ {765/763}, 26 $E_2'(10)$ {750/751}, 18 $E_1(10)$ {795/746}
B_u	767.5	6.00	764	w+	48 $E_1''(9)$ {760/758}, 26 $E_2'(11)$ {768/769}, 22 $E_2'(10)$ {750/751}
B_u	776.5	2.51	769	w	86 $E_2'(12)$ {773/784}
B_u	846.3	53.84	835	s	26 $E_1(11)$ {835/854}, 18 $E_2''(9)$ {765/763}, 18 $E_2'(11)$ {768/769}
B_u	849.4	21.06	835	s	72 $E_1(11)$ {835/854}
B_u	901.6	3.88	898	w+	78 $E_1(12)$ {911/906}
B_u	942.4	8.57	944	w+	92 $E_2'(13)$ {946/945}
B_u	1048.7	11.57	1040	w+	50 $E_2'(14)$ {1070/1064}, 22 $A_1'(7)$ {1060/1061}, 14 $E_1''(11)$ {1048/1057}
B_u	1057.0	18.34	1048	m	38 $E_1''(11)$ {1048/1057}, 32 $E_2'(14)$ {1070/1064}, 20 $A_1'(7)$ {1060/1061}
B_u	1063.5	8.59	1065	w	82 $E_2''(12)$ {1076/1070}, 12 $A_1'(7)$ {1060/1061}
B_u	1078.5	4.39	1077	w	82 $E_1(13)$ {1087/1082}
B_u	1116.0	16.80	1119	m	70 $A_2''(6)$ {1133/1130}
B_u	1134.7	9.19	1137	w+	22 $A_2''(6)$ {1133/1130}, 22 $E_1(14)$ {1176/1174}, 12 $E_2''(13)$ {1152/1160}, 12 $E_2'(15)$ {1196/1179}
B_u	1153.5	13.23	1149	w+	70 $E_2''(13)$ {1152/1160}, 22 $E_1(14)$ {1176/1174}
B_u	1168.7	32.36	1171	m	54 $E_2'(15)$ {1196/1179}, 16 $E_1''(12)$ {1172/1164}, 12 $A_1'(8)$ {1182/1174}, 10 $E_1(14)$ {1176/1174}
B_u	1171.9	11.04	1180	m	84 $A_1'(8)$ {1182/1174}
B_u	1213.2	4.02	1209	w+	40 $A_2''(7)$ {1203/1210}, 26 $E_1''(13)$ {1222/1214}, 22 $A_2'(7)$ {1215/1212}
B_u	1223.6	5.09	1226	w+	30 $A_1'(9)$ {1227/1227}, 22 $E_1(15)$ {1251/1243}, 12 $E_1''(13)$ {1222/1214}, 12 $E_2'(16)$ {1258/1253}
B_u	1235.6	18.80	1233	ms	50 $A_1'(9)$ {1227/1227}, 44 $E_1(15)$ {1251/1253}
B_u	1243.9	7.68	1245	w+, br	70 $E_2''(14)$ {1248/1246}, 24 $E_2'(16)$ {1258/1253}
B_u	1248.6	11.70	1250	w+, br	30 $E_2'(16)$ {1258/1253}, 26 $E_1(15)$ {1251/1243}, 14 $A_1'(9)$ {1227/1227}
A_u	1283.6	2.37	1287	m, br	60 E_1"(14) {1296/1294}
B_u	1286.5	5.97	1287	m, br	42 $E_1''(14)$ {1296/1294}, 34 $E_1(16)$ {1291/1292}
B_u	1290.4	14.76	1287	m, br	44 $E_1(16)$ {1291/1292}, 44 $E_1''(14)$ {1296/1294}
B_u	1311.3	9.51	1315	w	50 $E_2''(15)$ {1302/1311}, 22 $E_2'(17)$ {1332/1324}
B_u	1318.7	12.94	1326	w	66 $E_1(17)$ {1320/1320}, 24 $E_1''(15)$ {1310/1318}
B_u	1348.2	27.51	1350	w+	78 $E_2'(18)$ {1348/1345}
B_u	1373.4	25.92	1381	m	82 $E_2'(19)$ {*1374*/1356}
B_u	1388.2	54.49	1390	m	52 E_2"(17) {1400/1393}
A_u	1410.7	10.75	1409	w	44 $E_1(18)$ {1414/1406}, 26 $E_1(19)$ {1489/1475}, 12 E_1"(17) {1435/1429}
B_u	1444.0	100.00	1446	s	84 $E_2''(18)$ {1455/1446}
B_u	1467.4	10.19	1465	w, br	58 $A_1'(11)$ {1467/1467}, 12 $E_1(19)$ {1430/1430}
B_u	1469.3	4.13	1465	w, br	76 $E_1(20)$ {1489/1475}
B_u	1471.3	3.91	1465	w, br	42 $A_2''(9)$ {1460/1463}, 16 $E_1(20)$ {1489/1475}, 10 $A_1'(11)$ {1467/1467}
B_u	1488.6	13.88	1493	m	44 $E_2'(20)$ {1500/1491}, 28 $A_2''(9)$ {1460/1463}, 20 $A_1'(11)$ {1467/1467}
B_u	1498.3	6.31	1507	m	30 $E_2'(20)$ {1500/1491}, 22 $E_1''(18)$ {1511/1503}, 12 $E_2'(21)$ {1520/1510}
B_u	1519.4	34.98	1519	ms	18 $E_2'(21)$ {1520/1510}, 18 $E_1(21)$ {1557/1552}, 16 $E_2''(20)$ {−/1556}, 14 $E_1''(18)$ {1511/1503}, $E_2'(22)$ {1545/1555}
B_u	1548.9	42.59	1550	ms	32 $E_1(21)$ {1557/1552}, 32 $A_1'(12)$ {1564/1559}, 20 $A_2''(10)$ {1563/1553}
B_u	1556.2	23.14	1560	m	54 $A_1'(12)$ {1564/1559}, 28 $A_2''(10)$ {1563/1553}, 10 $E_1''(19)$ {*1564*/1557}
A_u	1563.3	6.47	sh		56 $E_2'(22)$ {1545/1555}, 14 $E_2''(20)$ {−/1556}, 12 E_1"(19) {1564/1557}

[a] A full list of calculated frequencies of the dimer is given in the Supporting Information, Table S1. [b] Calculated IR intensities are in %, 100% is the B_u mode at 1444 cm^{-1} (calcd). [c] Experimental intensities are w (weak) < w+ < m (medium) < ms (medium-strong) < s (strong), br (broad), "C_{70}" marks the modes in which frequencies coincide with C_{70} modes and hence their assignment to the dimer is somewhat ambiguous; [d] assignment in terms of C_{70} normal modes results from projection analysis, % of C_{70} vibration is given for each vibration of the dimer (contributions less than 10% are omitted), for C_{70} modes the values in brackets are experimental/calculated frequencies, the full list of C_{70} vibrational frequencies is given in Supporting Information, S2

either from IR or, in rare cases, from Raman-active modes of C_{70} (Table 3). In particular, the majority of intense IR modes of C_{70} have a counterpart in the spectrum of $[(C_{70})_2]^{2+}$ with medium to strong intensity. In the dimer the frequencies of C_{70} modes are almost the same, shifting normally to the higher frequencies by 2−6 cm^{-1}. However, there are two important exclusions from these relations. The first one is the $E_1'(10)$ mode of C_{70} at 795 cm^{-1}, which can be described as the out-of-plane vibrations of benzene rings on the equator of the C_{70} molecule. There is no intense counterpart for this mode in the spectrum

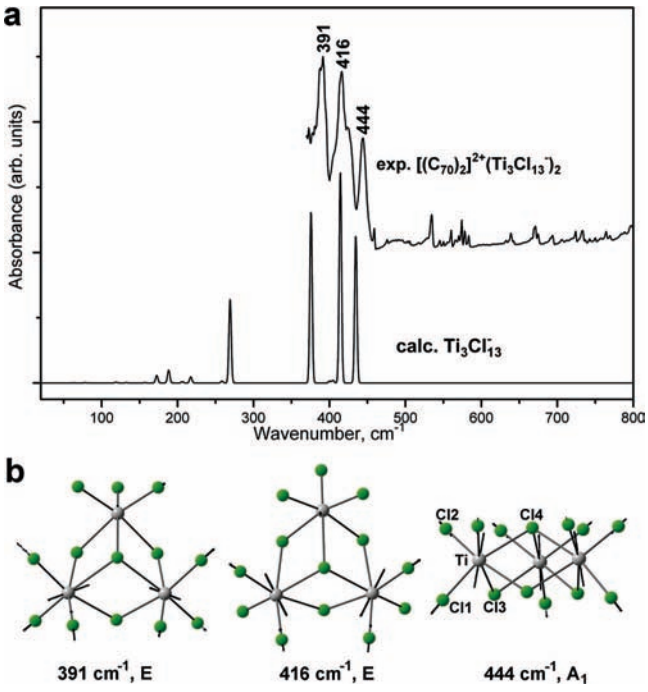

Figure 5. (a) IR absorption spectrum of $[(C_{70})_2]^{2+}(Ti_3Cl_{13})^-_2$ in the low-frequency range compared to the DFT-computed IR spectrum of $Ti_3Cl_{13}^-$; (b) vibrational atomic displacements for the most intense IR modes of $Ti_3Cl_{13}^-$.

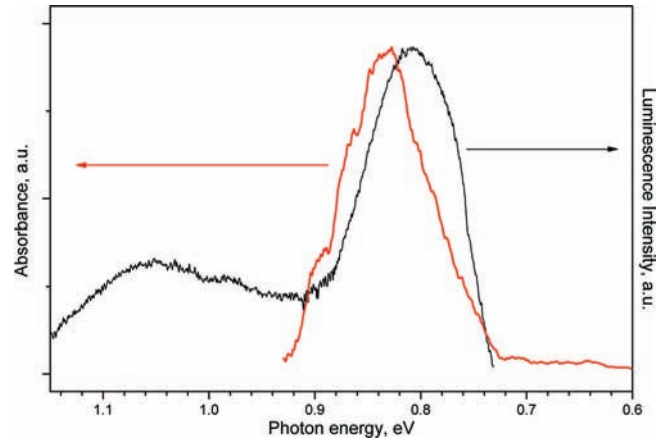

Figure 6. Absorption (red) and luminescence (black) spectra of $[(C_{70})_2]^{2+}(Ti_3Cl_{13})^-_2$ in the NIR range.

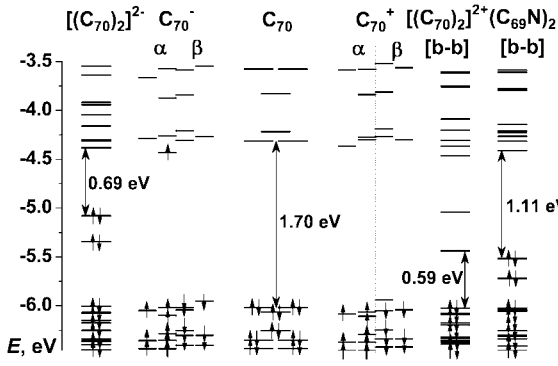

Figure 7. Frontier Kohn−Sham MO levels in single-bonded dimers, C_{70}, and its ions as computed at the PBE/TZ2P level. For the open shell structures, α and β spin levels are shown separately.

of $[(C_{70})_2]^{2+}$, and projection analysis has shown that this mode is strongly mixed with other C_{70} vibrations so that its contributions are scattered over the 200 cm^{-1} range in the spectrum of the dimer showing weak to negligible absorption intensities. Another exclusion is the $E_1'(19)$ at 1430 cm^{-1}, the strongest IR mode of C_{70}. Calculations showed that intensity of the corresponding vibrations in the dimer is very weak. Instead, the strong band at 1446 cm^{-1} in the IR spectrum of $[(C_{70})_2]^{2+}$ is caused by the silent fundamental of C_{70} $E_2''(18)$ (calcd 1446, exptl 1455 cm^{-1}). Note that it would be impossible to make this conclusion without projection analysis, and thus a wrong assignment of the dimer band at 1446 cm^{-1} to the $E_1'(19)$ mode of C_{70} could be proposed.

Vibrational Modes of $Ti_3Cl_{13}^-$. In addition to the cationic dimer of C_{70}, $[(C_{70})_2]^{2+}(Ti_3Cl_{13})^-_2$ also affords a new chlorotitanate anion, $Ti_3Cl_{13}^-$, which has never been observed in other Ti−Cl systems. This encouraged us to study its vibrational spectrum as well. Idealized symmetry of $Ti_3Cl_{13}^-$ is C_{3v}, its vibrations span $9A_1 + 5A_2 + 14E$ symmetry types, of which A_1 and E modes are IR active. Figure 5 compares the computed IR spectrum of $Ti_3Cl_{13}^-$ to the spectrum of the complex in the low-frequency range. DFT predicts that the cluster vibrations occur in the range of 40−440 cm^{-1}, and thus only a fraction of $Ti_3Cl_{13}^-$ modes is accessible experimentally. However, the most intense bands at 391, 416, and 444 cm^{-1} are within the limits of our spectrometer and by comparison to the DFT-computed spectrum they can be readily assigned to the vibrational modes of the anion at 376 (E), 414 (E), and 435 cm^{-1} (A_1), respectively, whose vibrational displacements are shown in Figure 5 (note that IR intensities of the anion vibrations are several times higher than absorption intensities of the fullerene part). Analysis of the potential energy distribution has shown that these vibrations can be described as stretches of the terminal Ti−Cl bonds. Their averaged experimental bond length is 2.208 Å,[2] while theory yields 2.233 Å for Ti−Cl1 and 2.244 Å for Ti−Cl2 (see Figure 5 for the numbering of chlorine atoms). Bridging Ti−μ^2-Cl3 bonds as well as Ti−μ^3-Cl4 bonds are considerably longer (exptl 2.483 and 2.578 Å, calcd 2.512 and 2.655 Å, respectively), and their vibrations are expected at lower frequencies with a gap of 100 cm^{-1} (see Table S3 in the Supporting Information). For instance, the intense IR band at 271 cm^{-1} is largely due to the stretching vibration of the Ti−μ^2-Cl3 bonds. To our knowledge, no other Ti−Cl system except for the $TiCl_4$ and its complexes has been studied by vibrational spectroscopy.[32] In the liquid $TiCl_4$, the IR active stretching Ti−Cl mode is observed at 490 cm^{-1} (DFT yields 489 cm^{-1}), while in $TiCl_4 \cdot 2L$ complexes (L = monodentate ligand) with hexacoordinated Ti this mode is shifted to ca. 380 cm^{-1} reflecting elongation of Ti−Cl bond lengths with the increase of the Ti coordination number.[32] The DFT-optimized Ti−Cl bond length in $TiCl_4$ is 2.192 Å, while in the crystalline $TiCl_4$ the average Ti−Cl bond is 2.163 Å long. Thus, the Ti−Cl bond in $TiCl_4$ is somewhat shorter that terminal Ti−Cl bonds in the $Ti_3Cl_{13}^-$ anion, in agreement with the higher Ti−Cl stretching frequency in $TiCl_4$.

Electronic Structure of $[(C_{70})_2^{2+}]$ and Other Single-Bonded Dimmers. Charged fullerenes, either in the anionic or cationic forms, exhibit characteristic absorptions in the near-infrared (NIR) range,[9] which are attributed to the SOMO → LUMO+N and HOMO−N → SOMO excitations, respectively. For instance, in the C_{70}^- spectrum the NIR band is observed at 1373 nm[9] and is assigned to the SOMO → LUMO+4 excitation.[33] The data on C_{70}^+ are more ambiguous largely because its NIR bands are substantially less intense while the cation is very unstable. Bolskar observed an absorption at 780 nm,[9] and this observation agrees with the absorption spectrum of C_{70}^+ generated in the neon matrix.[34] Our time-dependent DFT

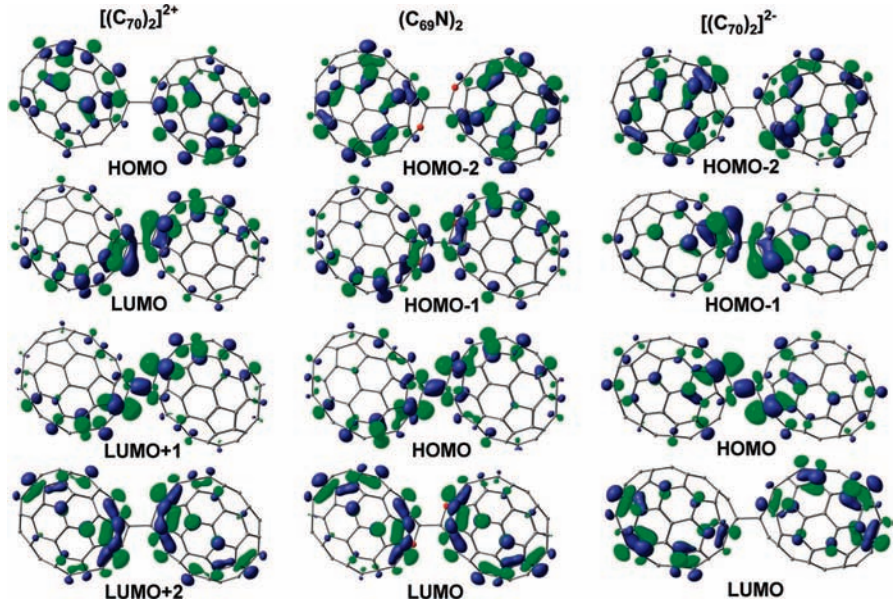

Figure 8. Frontier MOs in $[(C_{70})_2]^{2+}$ (left), isostructural $(C_{69}N)_2$ (middle), and $[(C_{70})_2]^{2-}$ (right).

calculations have shown that the band at 780 nm could be assigned to the HOMO−10 → SOMO excitation predicted at 1.46 eV (851 nm); however, calculations also predict more intense absorption at 0.76 eV (1641 nm), which was not observed experimentally (see the Supporting Information, Table S4). Dimerization of the ion-radicals should certainly affect NIR transitions. For instance, Konarev et al. found two prominent NIR absorptions at 910 and 1240 nm in the absorption spectrum of $[(C_{70})_2{}^{2-}]$ as opposed to the one NIR band of $C_{70}{}^-$.[35] To reveal the effect of the dimerization on the cation, we have studied the spectra of the complex in the NIR range. Figure 6 shows the absorption spectrum of the sample (limited to the energy range below 7000 cm^{-1}), superimposed on the luminescence spectrum excited with the 1064 nm line of a Nd:YAG laser. In both spectra one can see the band at 0.9−0.8 eV, which may be assigned to the HOMO−LUMO transitions in $(C_{70})_2{}^{2+}$, and through the intercrossing of the absorption and luminescence spectra, the band gap of the dimer is estimated as 0.82 eV in reasonable agreement with the DFT-predicted value of 0.59 eV (note that DFT without exact exchange admixture usually underestimates the HOMO−LUMO gap). The DFT-predicted HOMO−LUMO gap of the $Ti_3Cl_{13}{}^-$ anion is 2.35 eV, and thus the NIR band is undoubtedly attributed to the dimeric fullerene cation.

To reveal the nature of the NIR bands in single-bonded dimers of C_{70} we have analyzed their electronic structure in comparison to that of the radical anion and cation of C_{70} at the DFT level of theory. MO energy levels of the dimers are shown and compared to those of C_{70} in Figure 7 (note that the energy levels of charged species are shifted to the higher (cations) or lower (anions) energies to be seen on the same scale with C_{70}). One can see that in the radical anion and cation of C_{70} the α and β electrons exhibit somewhat different energies while *E*-symmetry orbitals are split, but degree of splitting is rather small, and the structure of MO levels in both the cation and the anion is similar to that of the neutral C_{70}. However, the electronic structure of the dimers is markedly different. All dimers exhibit two specific MO levels which have no analogues in the C_{70} and its radical anion or cation. In the anionic dimer these levels are occupied, while in the cationic dimer both are vacant. In the energy scale these levels are located in the middle of the HOMO−LUMO gap of C_{70}, and hence electron excitations to and from these levels are responsible for the NIR absorptions in $[(C_{70})_2]^{2+}$ and $[(C_{70})_2]^{2-}$, respectively. Figure 8 visualizes corresponding MOs of the dimers. Both MOs exhibit a considerable degree of localization close to the intercage bond and can be described as symmetric and antisymmetric superposition of the same MO pattern of the monomeric unit. The orbital with symmetric superposition (A_g), which is LUMO+1 in $[(C_{70})_2]^{2+}$ and HOMO in $[(C_{70})_2]^{2-}$, has considerable bonding nature for the intercage bond, while the "antisymmetric" orbital (B_u), which is LUMO in $[(C_{70})_2]^{2+}$ and HOMO−1 in $[(C_{70})_2]^{2-}$, has an antibonding character for this bond. Further analysis of the spatial localization of other frontier orbitals in $[(C_{70})_2]^{2+}$ and $[(C_{70})_2]^{2-}$ has shown that they are largely reminiscent of C_{70} MOs.

Significantly, the shapes of the characteristic MOs are almost the same in the cationic and anionic dimers, even though they are linked through the different carbon atoms. Moreover, the orbitals analogous to the HOMO of $[(C_{70})_2]^{2-}$ and LUMO+1 of $[(C_{70})_2]^{2+}$ were earlier found in $[(C_{60})_2]^{2-}$ and $(C_{59}N)_2$.[36] The presence of two specific electronic levels in $[(C_{60})_2]^{2-}$ separated from all other orbitals was also confirmed by photoelectron

TABLE 4: DFT Relative Energies (ΔE, kJ·mol^{-1}) and Inter-Cage Bond Lengths (d_{C-C}, Å) in the Isomers of $[(C_{70})_2]^{2+}$, $[(C_{70})_2]^{2-}$, and $(C_{69}N)_2$ Dimers

	$[(C_{70})_2]^{2+}$		$[(C_{70})_2]^{2-}$		$(C_{69}N)_2$[a]			$C_{69}N$[c]
	ΔE	d_{C-C}	ΔE	d_{C-C}	ΔE	d_{C-C}	C→N	ΔE
[a−a]	46.6	1.668	0.0	1.634	0.0	1.593	b	3.1
[b−b]	0.0	1.647	55.4	1.657	37.6	1.597	a	6.6
[c−c]	15.6	1.667	43.1	1.647	26.3	1.602	c	0.3
[d−d]	5.2	1.679	32.5	1.663	95.9	1.621	d	0.0
[e−e]	—[d]	—[d]	146.6	1.650	147.1	1.628	d	0.0
[2+2] [e]	13.8		35.6					

[a] In $(C_{69}N)_2$ dimers **[a−a]** means that $C_{69}N$ units are linked through C atoms of **a** type, just like for $(C_{70})_2$. [b] This column shows which carbon atom in C_{70} (closest to the C-sp^3 atom) is replaced by nitrogen; for **[d−d]** and **[e−e]** the position of nitrogen is not obvious, and hence several isomer were computed and the values listed in the table correspond to the lowest energy isomers. [c] Relative energies of $C_{69}N$ radicals corresponding to the dimers; that is, the line **[a−a]** contains the data on the isomer of $C_{69}N$ in which N replaces one of the carbon atoms of **b** type. [d] Bonded state for the dimer was not found. [e] [2+2] denotes the structure found for the neutral $(C_{70})_2$ dimer (Figure 1d).

TABLE 5: Spin Population in the DFT-Optimized Structures of C_{70}^+ and C_{70}^-

	C_{70}^+		C_{70}^-	
	per atom [a]	net [b]	per atom	net
a	−0.001, 0.014, 0.005	0.073	0.100, −0.011, 0.057	0.385
b	−0.023, 0.000, −0.014	−0.103	0.018, −0.001, 0.012	0.081
c	0.073, −0.026, 0.010, 0.070, 0.014	0.569	0.019, −0.008, 0.018, 0.035, −0.008	0.226
d	0.015, 0.071, 0.010, −0.022, 0.070	0.577	0.013, 0.046, 0.005, −0.015, 0.050	0.396
e	−0.005, −0.026, −0.007, 0.005, −0.023	−0.105	−0.005, −0.018, −0.006, 0.002, −0.017	−0.090

[a] The values are listed in the order **a1**, **a2**, **a3**, etc. Positions of **a1**, **b1**, etc. are shown in Figure 4; other atoms of the same type are numbered in the clock-wise direction. [b] The values summed up for all atoms of the given type.

spectroscopy,[11] which showed a distinct two-band feature in the vicinity of the highest occupied orbitals. Thus, we conclude that such orbitals can be considered as a characteristic feature of all single-bonded dimers of fullerenes. It is also instructive to compare the electronic structure of the charged C_{70} dimers to that of $(C_{69}N)_2$. Though the shape of characteristic orbitals in the latter is similar to that in $[(C_{70})_2]^{2+}$ and $[(C_{70})_2]^{2-}$ (Figure 8), HOMO and HOMO−1 in $(C_{69}N)_2$ are considerably stabilized (i.e., their energies are lowered with respect to the energies of all other orbitals). The same phenomenon was also observed for $(C_{59}N)_2$, both experimentally by photoelectron spectroscopy[37,38] and theoretically by DFT calculations.[36] It can be attributed to the stabilizing effect of the additional positive charge on the nitrogen sites.

Structural Peculiarities of the Charged Dimers of C_{70}. C_{70} has five symmetry inequivalent atoms thus allowing a possibility of 15 different isomers of the single-bonded dimers. Given the five symmetry inequivalent atoms of C_{70} are labeled **a** to **e** from the top to the equator of the molecule (Figure 4), the experimentally available $[(C_{70})_2]^{2+}$ and $[(C_{70})_2]^{2-}$ isomers can be designated as $[\mathbf{b}-\mathbf{b}]^{2+}$ and $[\mathbf{a}-\mathbf{a}]^{2-}$, and this designation will be used in the following discussion. Note also that both **a** and **b** atoms are involved in the formation of the intercage bonds in the neutral $(C_{70})_2$ dimer.[24] Our calculations have shown that the isomers with the opposite bond motifs, i.e. $[\mathbf{a}-\mathbf{a}]^{2+}$ and $[\mathbf{b}-\mathbf{b}]^{2-}$, are less stable then experimentally available structures $[\mathbf{b}-\mathbf{b}]^{2+}$ and $[\mathbf{a}-\mathbf{a}]^{2-}$ by 46.6 and 55.4 kJ·mol^{-1}, respectively. This shows that the stability of the single-bonded dimers can be substantially dependent on the bonding sites, and to obtain deeper insight into this problem we have checked all possible bonding motifs for $[(C_{70})_2]^{2+}$ and $[(C_{70})_2]^{2-}$. Table 4 lists relative energies for all symmetric dimers (i.e., the dimers in which monomers are linked by the atoms of the same type). The energies of the "mixed" type dimers (e.g., $[\mathbf{a}-\mathbf{b}]^{2+}$, etc.) were found to be well approximated by the mean value of the energies of two symmetric motifs (e.g., $\Delta E_{[\mathbf{a}-\mathbf{b}]} \approx 0.5(\Delta E_{[\mathbf{a}-\mathbf{a}]} + \Delta E_{[\mathbf{b}-\mathbf{b}]})$ within 2−3 kJ·mol^{-1}), and these values will not be discussed here in detail (see Table S5 in the Supporting Information). It is remarkable that for both cationic and anionic dimers, the experimental structures correspond to the lowest energy isomers. However, while the $[\mathbf{a}-\mathbf{a}]^{2-}$ isomer of the anionic dimer is substantially more stable than all other structures, the $[\mathbf{d}-\mathbf{d}]^{2+}$ isomer of the dimeric dication is only 5.2 kJ·mol^{-1} less stable than the experimentally determined structure of $[(C_{70})_2]^{2+}$. Furthermore, optimization of the mixed $[\mathbf{b}-\mathbf{d}]^{2+}$ isomer revealed that it is only 2 kJ·mol^{-1} less stable than the $[\mathbf{b}-\mathbf{b}]^{2+}$ isomer.

To shed the light on the reasons for such a strong dependence of the dimer stability on the bonding site, we have studied the structures of the preceding radical-ions C_{70}^+ and C_{70}^- in more detail. First, it is natural to consider that dimerization should occur through the sites with the highest spin density, and thus the spin density distribution in C_{70}^+ and C_{70}^- was analyzed. DFT-computed spin populations in these radical-ions are listed in Table 5, while the spatial distribution of the spin density is shown in Figure 9. On the other hand, all fullerenes suffer inherit curvature-induced strain, and it is considered that the atoms with the highest curvature are most prone to the chemical modification.[39] A convenient measure of the local curvature (deviation from planarity) for a given carbon atom is provided by the π-orbital axis vector (POAV) analysis.[40] In this approach, the π-orbital vector is postulated to make equal angles, $\theta_{\sigma\pi}$, to three σ bonds, and pyramidalization angle is defined as $(\theta_{\sigma\pi} - 90°)$. Larger $(\theta_{\sigma\pi} - 90°)$ values correspond to the higher curvature-induced strain. Table 6 lists $(\theta_{\sigma\pi} - 90°)$ values for C_{70}, C_{70}^+, and C_{70}^-. Note that the cation and anion both have only C_{2v} symmetry due to Jahn−Teller distortion.

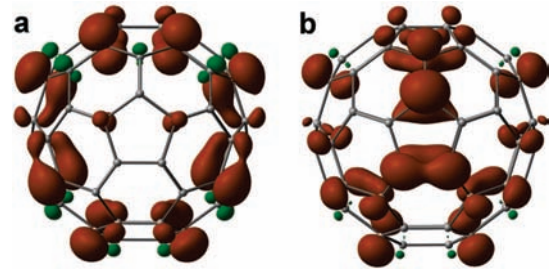

Figure 9. Spatial distribution of the spin density in C_{70}^+ (a) and C_{70}^- (b).

Analysis of the data in Tables 5 and 6 shows that the highest spin density in the monoanion is located on the **a1** atom, which is lying on the symmetry plane. The net spin population on **a** atoms is comparable to that of the atoms of **d**-type; however, when the values for individual atoms are considered, spin population on the **a1** is found to be two or more times larger than that on the other atoms. Moreover, the **a1** atom also has the largest $(\theta_{\sigma\pi} - 90°)$ value, 12.34° (for comparison, the value for the atoms of **a**-type in neutral C_{70} is 11.83°). Thus, dimerization of C_{70}^- through the **a**−**a** bond formation is favored by both spin density and local curvature, which explains why $[\mathbf{a}-\mathbf{a}]^{2-}$ is considerably more stable than all other isomer of $[(C_{70})_2]^{2-}$. The largest POAV values in the C_{70}^+ cation are found for the atoms of **b** type, and this is a probable explanation of the higher stability of the $[\mathbf{b}-\mathbf{b}]^{2+}$ dimer. However, the spin density distribution in the cation is substantially different than that in the anion (Figure 9), the largest spin density corresponding to the atoms of **c** and **d** types. As a result, $[\mathbf{c}-\mathbf{c}]^{2+}$ and $[\mathbf{d}-\mathbf{d}]^{2+}$ isomers appear to be much closer in energy to the $[\mathbf{b}-\mathbf{b}]^{2+}$ than respective isomers of the anionic dimer.[41] Note that POAV analysis explains the very low stability of the $[\mathbf{e}-\mathbf{e}]^{2-}$ dimer by the small pyramidalization angle for **e** atoms (for the cationic dimer, this isomer did not provide a bounded state at all), which is in line with the avoidance of the **e** atoms in C_{70} and atoms at the triple hexagon junctions in general in the chemical derivatization of higher fullerenes.[42−46] Finally, it is worth noting that the lowest energy isomers of $[(C_{70})_2]^{2+}$ and

TABLE 6: POAV Pyramidalization Angles ($\theta_{\sigma\pi} - 90°$) in the DFT-Optimized Structures of C_{70}, C_{70}^+, and C_{70}^-

	C_{70}	$C_{70}^{+\,a}$	$C_{70}^{-\,a}$
a	11.83	11.88, 11.75, 11.82	12.34, 11.56, 12.0
b	11.96	12.11, 12.07, 12.10	12.06, 11.81, 11.98
c	11.48	11.27, 11.67, 11.43, 11.20, 11.56	11.56, 11.28, 11.42, 11.60, 11.36
d	10.21	10.25, 9.96, 10.12, 10.31, 10.05	10.25, 10.38, 10.13, 10.05, 10.45
e	8.59	8.73, 8.70, 8.66, 8.68, 8.74	8.58, 8.51, 8.48, 8.51, 8.58

[a] The values are listed in the order **a1**, **a2**, **a3**, etc. Positions of **a1**, **b1**, etc. are shown in Figure 4; other atoms of the same type are numbered in the clock-wise direction.

$[(C_{70})_2]^{2-}$ have the shortest DFT-optimized intercage bond lengths in each set of possible isomers.

It is instructive to compare the relative energies of $[(C_{70})_2]^{2-}$ isomers to those of the isoelectronic $(C_{69}N)_2$ dimer (Table 4). Similar to the $[(C_{70})_2]^{2-}$, the [**a**−**a**] isomer is favored for the $(C_{69}N)_2$ followed by the [**c**−**c**] and [**b**−**b**] isomers; however, the latter exhibit higher relative stability than for the anionic dimer (26.3 and 37.6 kJ·mol^{-1} vs 43.1 and 55.4 kJ·mol^{-1}, respectively, see Table 4). In contrast to the $[(C_{70})_2]^{2-}$ represented by the single $[\mathbf{a}-\mathbf{a}]^{2-}$ isomer, three symmetric [**a**−**a**], [**b**−**b**],[17,18] and [**c**−**c**][16] isomers as well as the mixed [**a**−**b**] isomer[17] of $(C_{69}N)_2$ were isolated. In similar synthetic conditions [**b**−**b**] is usually obtained in much higher yield; however, as follows from our results, it is only a kinetic product, and the relative yields of $(C_{69}N)_2$ isomers are largely determined by the stability of the intermediates. Note that just as in the $[(C_{70})_2]^{2-}$, the shortest intercage C−C bond in $(C_{69}N)_2$ also corresponds to the most stable isomer. However, the intercage bonds in the azafullerene dimers are systematially 0.04−0.06 Å shorter than in the charged single-bonded dimers of C_{70} (Table 4). The same difference in the bond lengths was reported for $(C_{59}N)_2$ and $[(C_{60})_2]^{2-}$ in ref 36 (see also Table 4 for the results computed in this work).

Binding Energies. The last column in Table 2 lists dimerization energies E_{dim} for the dimers (a positive value means that the dimer is unstable with respect to the decomposition into monomeric species). As could be anticipated, both cationic and anionic dimers of C_{70} are significantly unstable (E_{dim} = ca. 100 kJ/mol), which can be explained by a domination of the Coulomb repulsion (E_{Coul}) in the intercage interactions,[36] and hence formation of the charged dimers is possible only in the presence of the counterions which compensate for the strong Coulomb repulsion between the monomeric units. E_{Coul} can be roughly estimated as a repulsion energy of the two point charges located in the centers of mass of the monomeric units, which amounts to 136.3 kJ/mol for $[\mathbf{b}-\mathbf{b}]^{2+}$. Probably a more accurate estimation can be done by using Hirschfield atomic charges from DFT calculations and summing up all pairwise interatomic interactions between different monomeric units. For $[\mathbf{b}-\mathbf{b}]^{2+}$ this approach yields 146.6 kJ/mol, and almost the same values within 3−4 kJ/mol are obtained for all other isomers of $[(C_{70})_2]^{2+}$ in spite of the fact that they have different intercage distances. The latter can be explained by the fact that the distribution of excess charge in single-bonded dimers is mostly governed by the frontier orbitals associated with the intercage bonds (see Figure 8). As these orbitals have identical shapes in all isomers, E_{Coul} computed by this method is almost the same for all isomers. Calculated values can be compared to the experimentally measured Hubbard U value in $(C_{59}N)_2$ recently reported by Schulte et al.[38] U in $(C_{69}N)_2$ can be interpreted as the energy of the Coulomb repulsion in $[(C_{59}N)_2]^{2+}$ and is estimated as 106 kJ/mol for the HOMO to 130 kJ/mol for the deeper lying orbitals.[38] Recently Coulomb repulsion energy in the $C_{120}O^{2-}$ dimer was estimated as 0.8 eV by Wang et al.[47] Given E_{Coul} is subtracted from E_{dim}, the residue can be interpreted as the covalent contribution to E_{dim}, which turns out to be negative. However, the values are still much smaller than E_{dim} values predicted for $(C_{59}N)_2$ and $(C_{69}N)_2$, which can be explained by the longer intercage bonds in the charged dimers. Thus, Coulomb repulsion in the latter weakens covalent bonding between monomeric units.

Note that computed E_{dim} reasonably correlates with the experimental data on decomposition of the dimers. The least stable dimer according to the E_{dim} value, $[(C_{60})_2]^{2-}$, was shown to decompose at 160−250 K depending on the counterion,[35] decomposition of $[(C_{70})_2]^{2-}$ occurs at 250−360 K,[35] while for the $(C_{59}N)_2$ a substantial fraction of the dimer survived heating up to 750−830 K.[29,48] Given similar kinetic stability is proposed for the $[(C_{70})_2]^{2-}$ and $[(C_{70})_2]^{2+}$ dimers, the synthesis of the latter at 373 K (the temperature used in this work) is most probably a reversible process, and hence the thermodynamically stable $[\mathbf{b}-\mathbf{b}]^{2+}$ isomer is formed. It is yet to be seen if variation of reaction condition or quenching of the reaction mixture at a certain point can result in the formation of the kinetically more preferable $[\mathbf{d}-\mathbf{d}]^{2+}$ isomer of $[(C_{70})_2]^{2+}$.

Summary and Conclusions

The spectra, electronic structure, and energetics of the single-bonded cationic dimer of C_{70}, $[(C_{70})_2]^{2+}$, have been thoroughly studied experimentally and with the use of DFT calculations. The IR spectrum of the cationic dimer is reported for the first time and its interpretation in terms of the parent C_{70} fundamentals is fulfilled. It is shown that charging of C_{70} weakly affects its vibrational frequencies and eigenvectors, and so does the dimerization of the cation. Projection analysis revealed that majority of the strong IR active modes of C_{70} appear in the IR spectrum of the dimer with medium to strong intensity. At the same time, analysis of the IR spectra of all single-bonded dimers revealed a characteristic vibration of these species. In particular, in the IR spectra all single-bonded dimers exhibit a strong absorption in the 800−900 cm^{-1} range due to the specific vibration of the intercage bond.

In the electronic structure all single-bonded dimers are shown to have two specific orbitals, one of which is bonding while the other is antibonding for the intercage bond. These levels are lowest unoccupied in the cationic dimer or highest occupied in the anionic dimers as well as in the azafullerene dimers. In the energy scale these levels are located approximately in the middle of the HOMO−LUMO gaps of corresponding fullerenes, resulting in the small gaps of the single-bonded dimers and appearance of the NIR bands in the absorption spectra of the cationic and anionic dimers.

The study of the energetics of the possible isomers of single-bonded dimers of C_{70} revealed that experimentally observed structures of $[(C_{70})_2]^{2+}$ and $[(C_{70})_2]^{2-}$ are the most stable isomers. For the anionic dimer, formation of the experimentally observed isomer is favored by both spin density distribution and local

curvature of the carbon atoms (quantified in terms of POAV angles) in C_{70}^-. As a result, the experimentally observed isomer of $[(C_{70})_2]^{2-}$ is found to be significantly lower in energy than all other isomers. On the contrary, formation of the experimentally observed isomer of the cationic dimer is favored only by POAV values, while spin density distribution favors different isomers. As a result, the experimentally observed isomer of $[(C_{70})_2]^{2+}$ is only slightly more stable than the two other isomers, and their isolation can be expected in the future.

Acknowledgment. We thank Dr. Robert Bolskar for discussion of the absorption spectra of C_{70}^+, Dr. Karine Schulte for the discussion of Coulomb interaction in $(C_{59}N)_2$, and Mr. Frank Ziegs for assistance in Raman measurements. Financial support from the Alexander von Humboldt Foundation (to A.A.P.) and computer time at the Research Computing Center of MSU are gratefully acknowledged. We are also thankful to U. Nitzsche for technical assistance with the computer resources at IFW.

Supporting Information Available: DFT-optimized Cartesian coordinates of the dimer molecules, full list of DFT-computed vibrational frequencies and absorption intensities of $[(C_{70})_2]^{2+}$ and $Ti_3Cl_{13}^-$, full list of DFT-computed and experimental C_{70} fundamental frequencies, TD-DFT-computed lowest energy excitations in C_{70}^+ and C_{70}^-, and relative energies of the isomers of $[(C_{70})_2]^{2+}$. This material is available free of charge via the Internet at http://pubs.acs.org.

References and Notes

(1) Troyanov, S. I.; Popov, A. A. *Angew. Chem., Int. Ed.* **2005**, *44*, 4215.
(2) Troyanov, S. I.; Kemnitz, E. *Chem. Commun.* **2007**, 2707.
(3) Simeonov, K. S.; Amsharov, K. Y.; Jansen, M. *Angew. Chem., Int. Ed.* **2007**, *46*, 8419.
(4) Burtsev, A. V.; Kemnitz, E.; Troyanov, S. I. *Crystallogr. Rep.* **2008**, *53*, 639.
(5) Simeonov, K. S.; Amsharov, K. Y.; Jansen, M. *Chem.−Eur. J.* **2008**, *14*, 9585.
(6) Xie, Q. S.; Arias, F.; Echegoyen, L. *J. Am. Chem. Soc.* **1993**, *115*, 9818.
(7) Reed, C. A.; Kim, K. C.; Bolskar, R. D.; Mueller, L. J. *Science* **2000**, *289*, 101.
(8) Bolskar, R. D.; Mathur, R. S.; Reed, C. A. *J. Am. Chem. Soc.* **1996**, *118*, 13093.
(9) Reed, C. A.; Bolskar, R. D. *Chem. Rev.* **2000**, *100*, 1075.
(10) Oszlanyi, G.; Bortel, G.; Faigel, G.; Granasy, L.; Bendele, G. M.; Stephens, P. W.; Forro, L. *Phys. Rev. B* **1996**, *54*, 11849.
(11) Poirier, D. M.; Olson, C. G.; Weaver, J. H. *Phys. Rev. B* **1995**, *52*, 11662.
(12) Konarev, D. V.; Khasanov, S. S.; Vorontsov, I. I.; Saito, G.; Antipin, M. Y.; Otsuka, A.; Lyubovskaya, R. N. *Chem. Commun.* **2002**, 2548.
(13) Konarev, D. V.; Khasanov, S. S.; Vorontsov, I. I.; Saito, G.; Otsuka, A. *Synth. Met.* **2003**, *135*, 781.
(14) Konarev, D. V.; Khasanov, S. S.; Lyubovskaya, R. N. *Russ. Chem. Bull.* **2007**, *56*, 371.
(15) Vostrowsky, O.; Hirsch, A. *Chem. Rev.* **2006**, *106*, 5191.
(16) Tagmatarchis, N.; Okada, K.; Tomiyama, T.; Shinohara, H. *Synlett* **2000**, 1761.
(17) Nuber, B.; Hirsch, A. *Chem. Commun.* **1996**, 1421.
(18) BellaviaLund, C.; Wudl, F. *J. Am. Chem. Soc.* **1997**, *119*, 943.
(19) Perdew, J. P.; Burke, K.; Ernzerhof, M. *Phys. Rev. Lett.* **1996**, *77*, 3865.
(20) Laikov, D. N. *Chem. Phys. Lett.* **1997**, *281*, 151.
(21) Laikov, D. N.; Ustynuk, Y. A. *Russ. Chem. Bull.* **2005**, *54*, 820.
(22) Schettino, V.; Pagliai, M.; Cardini, G. *J. Phys. Chem. A* **2002**, *106*, 1815.
(23) Sun, G. Y.; Kertesz, M. *J. Phys. Chem. A* **2002**, *106*, 6381.
(24) Lebedkin, S.; Hull, W. E.; Soldatov, A.; Renker, B.; Kappes, M. M. *J. Phys. Chem. B* **2000**, *104*, 4101.
(25) Schober, H.; Renker, B. *Solid State Commun.* **1997**, *104*, 609.
(26) Lebedkin, S.; Gromov, A.; Giesa, S.; Gleiter, R.; Renker, B.; Rietschel, H.; Kratschmer, W. *Chem. Phys. Lett.* **1998**, *285*, 210.
(27) Plank, W.; Pichler, T.; Kuzmany, H.; Dubay, O.; Tagmatarchis, N.; Prassides, K. *Eur. Phys. J. B* **2000**, *17*, 33.
(28) Andreoni, W.; Curioni, A.; Holczer, K.; Prassides, K.; Keshavarz-K., M.; Hummelen, J. C.; Wudl, F. *J. Am. Chem. Soc.* **1996**, *118*, 11335.
(29) Krause, M.; Baes-Fischlmair, S.; Pfeiffer, R.; Plank, W.; Pichler, T.; Kuzmany, H.; Tagmatarchis, N.; Prassides, K. *J. Phys. Chem. B* **2001**, *105*, 11964.
(30) Martin, M. C.; Koller, D.; Rosenberg, A.; Kendziora, C.; Mihaly, L. *Phys. Rev. B* **1995**, *51*, 3210.
(31) Konarev, D. V.; Khasanov, S. S.; Otsuka, A.; Saito, G.; Lyubovskaya, R. N. *Inorg. Chem.* **2007**, *46*, 2261.
(32) Cooney, R. P.; Fraser, D. B. *Aust. J. Chem.* **1974**, *27*, 1855.
(33) Popov, A. A.; Shustova, N. B.; Boltalina, O. V.; Strauss, S. H.; Dunsch, L. *ChemPhysChem* **2008**, *9*, 431.
(34) Fulara, J.; Jakobi, M.; Maier, J. P. *Chem. Phys. Lett.* **1993**, *206*, 203.
(35) Konarev, D. V.; Khasanov, S. S.; Saito, G.; Otsuka, A.; Yoshida, Y.; Lyubovskaya, R. N. *J. Am. Chem. Soc.* **2003**, *125*, 10074.
(36) Andreoni, W. *Annu. Rev. Phys. Chem.* **1998**, *49*, 405.
(37) Hunt, M. R. C.; Pichler, T.; Siller, L.; Bruhwiler, P. A.; Golden, M. S.; Tagmatarchis, N.; Prassides, K.; Rudolf, P. *Phys. Rev. B* **2002**, *66*, 4.
(38) Schulte, K.; Wang, L.; Moriarty, P. J.; Prassides, K.; Tagmatarchis, N. *J. Chem. Phys.* **2007**, *126*, 6.
(39) Haddon, R. C. *Science* **1993**, *261*, 1545.
(40) Haddon, R. C.; Scott, L. T. *Pure Appl. Chem.* **1986**, *58*, 137.
(41) Note that the two factors considered cannot fully explain relative stabilities of the isomers: for instance, it is not clear at this time why the $[\mathbf{d}-\mathbf{d}]^{2+}$ isomer is more stable than $[\mathbf{c}-\mathbf{c}]^{2+}$ in view of the larger POAV values for the atoms of **c** type.
(42) Troyanov, S. I.; Kemnitz, E. *Eur. J. Org. Chem.* **2003**, 3916.
(43) Troyanov, S. I.; Kemnitz, E. *Eur. J. Org. Chem.* **2005**, 4951.
(44) Shustova, N. B.; Kuvychko, I. V.; Bolskar, R. D.; Seppelt, K.; Strauss, S. H.; Popov, A. A.; Boltalina, O. V. *J. Am. Chem. Soc.* **2006**, *128*, 15793.
(45) Kareev, I. E.; Kuvychko, I. V.; Shustova, N. B.; Lebedkin, S. F.; Bubnov, V. P.; Anderson, O. P.; Popov, A. A.; Boltalina, O. V.; Strauss, S. H. *Angew. Chem., Int. Ed. Engl.* **2008**, *47*, 6204.
(46) Kareev, I. E.; Popov, A. A.; Kuvychko, I. V.; Shustova, N. B.; Lebedkin, S. F.; Bubnov, V. P.; Anderson, O. P.; Seppelt, K.; Strauss, S. H.; Boltalina, O. V. *J. Am. Chem. Soc.* **2008**, *130*, 13471.
(47) Wang, X. B.; Matheis, K.; Ioffe, I. N.; Goryunkov, A. A.; Yang, J.; Kappes, M. M.; Wang, L. S. *J. Chem. Phys.* **2008**, *128*, 114307.
(48) Simon, F.; Arcon, D.; Tagmatarchis, N.; Garaj, S.; Forro, L.; Prassides, K. *J. Phys. Chem. A* **1999**, *103*, 6969.

JP805264Q